Global response of clear-air turbulence to climate change

AGU PUBLICATIONS

Geophysical Research Letters

RESEARCH LETTER
10.1002/2017GL074618

Key Points:
- Clear-air turbulence diagnosed from a climate model more than doubles in some locations by 2050–2080
- Locally, severe turbulence increases more than light and moderate turbulence
- The increases depend on altitude and are larger at 39,000 feet than 34,000 feet

Correspondence to:
L. N. Storer,
luke.storer@pgr.reading.ac.uk

Citation:
Storer, L. N., Williams, P. D., & Joshi, M. M. (2017). Global response of clear-air turbulence to climate change. *Geophysical Research Letters, 44*, 9976–9984. https://doi.org/10.1002/2017GL074618

Received 16 JUN 2017
Accepted 31 AUG 2017
Published online 3 OCT 2017

Global Response of Clear-Air Turbulence to Climate Change

Luke N. Storer[1], **Paul D. Williams**[1], **and Manoj M. Joshi**[2]

[1]Department of Meteorology, University of Reading, Reading, UK, [2]Climatic Research Unit, School of Environmental Sciences, University of East Anglia, Norwich, UK

Abstract Clear-air turbulence (CAT) is one of the largest causes of weather-related aviation incidents. Here we use climate model simulations to study the impact that climate change could have on global CAT by the period 2050–2080. We extend previous work by analyzing eight geographic regions, two flight levels, five turbulence strength categories, and four seasons. We find large relative increases in CAT, especially in the midlatitudes in both hemispheres, with some regions experiencing several hundred per cent more turbulence. The busiest international airspace experiences the largest increases, with the volume of severe CAT approximately doubling over North America, the North Pacific, and Europe. Over the North Atlantic, severe CAT in future becomes as common as moderate CAT historically. These results highlight the increasing need to improve operational CAT forecasts and to use them effectively in flight planning, to limit discomfort and injuries among passengers and crew.

Plain Language Summary Clear-air turbulence is potentially hospitalizing in-flight bumpiness experienced by aircraft. Often, pilots cannot avoid it, because it is invisible to the naked eye and undetectable by onboard sensors. Previous research suggests that climate change will increase instabilities in the North Atlantic jet stream in winter, generating more clear-air turbulence. This study analyzes changes to clear-air turbulence over the entire globe by the second half of this century. We consider eight geographic regions, two flight levels, five turbulence strength categories, and all four seasons. We find strong increases in clear-air turbulence over the entire globe and in particular the midlatitudes, which is where the busiest flight routes are. We also find that the strongest turbulence will increase the most, highlighting the importance of improving turbulence forecasts and flight planning to limit discomfort and injuries to passengers and crew.

1. Introduction

Clear-air turbulence (CAT) is defined as high-altitude aircraft bumpiness in regions devoid of significant cloudiness and away from thunderstorm activity (Chambers, 1955). Without warning, aircraft can be violently thrown about by CAT. Any unsecured objects and unbuckled passengers and crew can be tossed around the cabin, causing serious injuries and even fatalities (De Villiers & van Heerden, 2001). The part of the flight most prone to injuries from CAT is the cruising phase above 10,000 ft, because passengers and crew are often unbuckled (Sharman et al., 2006). Despite recent advances in our mechanistic understanding (Knox et al., 2008; McCann et al., 2012), CAT remains one of the largest causes of weather-related aviation accidents. CAT has been found to account for 24% of weather-related accidents (Kim & Chun, 2011) and turbulence more generally for 65% of weather-related accidents (Sharman et al., 2006). According to official statistics, around 45 passengers and crew are injured by turbulence on United States-operated airlines each year, although these injury rates may be grossly underestimated because not all injuries are reported (Sharman et al., 2006). Turbulence is by far the most common cause of serious injuries to flight attendants (Tvaryanas, 2003). A comprehensive overview of aviation turbulence has been presented recently by Sharman and Lane (2016).

An important source of CAT is strong vertical wind shear, which is prevalent especially within the atmospheric jet streams. The wind shear creates regions of low Richardson number (Ri), in which unstable Kelvin–Helmholtz waves can grow and ultimately break down into turbulence (Lane et al., 2012). There are several other important sources of CAT, including airflow over mountainous terrain (Lilly, 1978), the effects

of remote convection (Koch & Dorian, 1988; Uccellini & Koch, 1987), and loss of balance (Williams et al., 2003, 2005, 2008). In these cases, gravity waves are formed and may propagate far away from the source region, eventually producing turbulence remotely when they either break or induce shear instabilities.

Because CAT is invisible and cannot be foreseen by pilots or onboard radar, the aviation sector relies on operational turbulence forecasts that are produced using numerical models. Turbulence in the atmosphere is energized from the planetary scale down to less than 1 cm. The turbulent eddies that cause aviation turbulence, however, typically occur on a reduced set of scales from around 100 m to 1 km. Computer processing speeds are currently not sufficient to explicitly simulate motions on these scales (Sharman et al. 2006), except for a few detailed case studies (e.g. Lane et al., 2012). Therefore, diagnostic indices from numerical weather prediction models are used to identify and forecast regions likely to contain CAT. The diagnostics generally assume that the smaller-scale turbulence is formed as a result of conditions set by the large-scale flow. Commonly used indices include variant 1 of the Ellrod and Knapp turbulence index (TI1), which has been shown to forecast up to 75% of CAT (Ellrod & Knapp, 1992), the negative Richardson number (−Ri), the Colson–Panofsky index (Colson & Panofsky, 1965), the Brown index (Brown, 1973), and the potential vorticity. Some indices, such as the Richardson number, explicitly diagnose a physical mechanism in the atmosphere that is known to cause CAT and are rigorously derivable from the equations of fluid dynamics via a stability analysis. Others, such as the Ellrod and Knapp (1992) indices, are more empirical but have nevertheless been found to be skillful indicators of CAT.

Jaeger and Sprenger (2007) produced a Northern Hemisphere climatology of CAT diagnosed from ERA-40 reanalysis data covering the period 1958–2001. ERA-40 has a spectral resolution of T159 horizontally, which corresponds to approximately 90 km in the midlatitudes. A positive trend in moderate-or-greater (MOG) turbulence was found for the four indices that were calculated: TI1, Brunt–Väisälä frequency (N^2), Richardson number (Ri), and potential vorticity. These findings suggest that climate change may be increasing the occurrence of CAT. Jaeger and Sprenger (2007) also found maximum probabilities of MOG turbulence over the east and west coasts of North America, with other local maxima over the Himalayas, central Europe, eastern China, and the western parts of the North Atlantic and North Pacific.

Our current understanding of the response of CAT to climate change has been summarized by Williams and Joshi (2016) and is part of a package of work being carried out in the burgeoning research area of climate impacts on aviation (e.g., Coffel & Horton, 2015; Irvine et al., 2016; Karnauskas et al., 2011; Williams, 2016, 2017; Williams & Joshi, 2013). In particular, Williams and Joshi (2013) used climate model simulations to diagnose 21 different CAT indices and thereby study how a doubling of the atmospheric carbon dioxide (CO_2) concentration could impact the amount of CAT on transatlantic flights in winter at 200 hPa. The north Atlantic flight corridor is one of the busiest in the world, with more than 300 flights per day in each direction (Irvine et al., 2013). From the 21-member ensemble of CAT indices, Williams and Joshi (2013) calculated a 10–40% increase in the median strength of CAT and a 40–170% increase in the frequency of occurrence of MOG CAT in this region, in the doubled-CO_2 simulation compared to a preindustrial control run. This was the first study to calculate how climate change may impact CAT in the future. Williams (2017) subsequently extended the calculations to study the individual responses of light, moderate, and severe turbulence, finding large and significant increases in each case.

The present paper builds on these previous studies by using a current-generation climate model to calculate for the first time how the various strength categories of CAT are projected to change in different geographic regions across the globe, at multiple flight levels, and in all seasons. The methodology is stated in section 2, the results are presented in section 3, and the paper concludes with a discussion in section 4.

2. Methodology

We use climate simulations that were performed with the Met Office Hadley Centre HadGEM2-ES model (Jones et al., 2011), which forms part of the fifth Coupled Model Intercomparison Project (CMIP5) ensemble (Taylor et al., 2012). This is the only CMIP5 model for which 6-hourly output fields have been archived on a suitable set of upper-tropospheric and lower-stratospheric pressure levels. The 6-hourly snapshots resolve the diurnal cycle and are therefore expected to provide a better representation of wind shear than the daily mean CMIP3 fields used by Williams and Joshi (2013) and Williams (2017). The multiple pressure levels make it possible to calculate the vertical wind shear using second-order centered finite differences at both 200 hPa and 250 hPa, which correspond to typical cruising altitudes of approximately 12 km (39,000 ft or FL390) and 10 km

(34,000 ft or FL340), respectively. The atmosphere model has a horizontal grid spacing of 1.25° in latitude and 1.875° in longitude, giving 192 × 144 grid boxes globally, which is finer than the 2.0° by 2.5° CMIP3 model used by Williams and Joshi (2013) and Williams (2017).

Two HadGEM2-ES simulations are analyzed to calculate how climate change could impact CAT in the upper troposphere and lower stratosphere in future. Specifically, a preindustrial control simulation (picontrol) is compared with a climate change simulation using the Intergovernmental Panel on Climate Change (IPCC) Representative Concentration Pathway 8.5 (RCP8.5) (Flato et al., 2013). The picontrol run is a base state that uses constant preindustrial greenhouse gas concentrations to simulate the global climate before the industrial revolution. The RCP8.5 run assumes a net radiative forcing increase of 8.5 W m^{-2} by 2100 (Van Vuuren et al., 2011), which implies greenhouse gas concentrations equivalent to around 1,370 ppmv of CO_2. We analyze 30 years of data for the future period 2050–2080 from RCP8.5 compared to 30 years of historic data from picontrol.

The present study focuses on CAT generated by wind shear and loss of balance, disregarding mountain waves and remote convection. For consistency, we calculate the same basket of CAT diagnostics indices as Williams and Joshi (2013) and Williams (2017), except that we exclude the potential vorticity diagnostic because it was found to give unrealistic results. We define a threshold for each turbulence strength category and each CAT diagnostic in HadGEM2-ES, following Williams (2017). The thresholds are appropriate for a large, commercial airliner. The calibration is based on the cube root of the eddy dissipation rate, which is proportional to the vertical acceleration of an aircraft experiencing turbulence (MacCready, 1964), and it is implemented as follows. First, the probability distribution is calculated for each of the 20 CAT diagnostics, using 6-hourly global fields from the 30 year picontrol run of HadGEM2-ES in all seasons on a given pressure level. Then, the top 0.1% (99.9–100%) of the probability distribution for each diagnostic is taken to represent severe turbulence, the next 0.1% (99.8–99.9%) is moderate-to-severe turbulence, the next 0.2% (99.6–99.8%) is moderate turbulence, the next 0.5% (99.1–99.6%) is light-to-moderate turbulence, and the next 2.1% (97–91.1%) is light turbulence. It follows from these percentiles that 0.1% of the global atmosphere at aircraft cruising altitudes contains severe-or-greater turbulence, 0.4% contains moderate-or-greater turbulence, and 3.0% contains light-or-greater turbulence. Extreme turbulence is neglected because of its rarity. To calculate regions of CAT, every time an index exceeds one of the above threshold values, it is classed as a turbulence event.

3. Results

As an initial check on the similarity between turbulence increases in different climate models, Figure 1 shows a scatterplot of the percentage change in the prevalence of MOG CAT in the north Atlantic in winter, as calculated from the CMIP3 GFDL-CM2.1 model used by Williams and Joshi (2013) and the CMIP5 HadGEM2-ES model used in the present study. To ensure a fair comparison, the 6-hourly wind and temperature fields from HadGEM2-ES are first time averaged to match the daily mean fields from GFDL-CM2.1, before calculating the CAT diagnostics. There is a clear correlation between changes in MOG CAT in the two models, as indicated by the correlation coefficient of 0.69. Most of the indices (18 out of 20) appear in the upper-right quadrant of the Cartesian plane, indicating increases in both models, although there is some scatter around the line of best fit.

Figure 1 shows that the CAT increases in HadGEM2-ES are on average 30% smaller than in GFDL-CM2.1, possibly because of the different anthropogenic forcing used in the climate change simulations. Specifically, the GFDL-CM2.1 climate change simulation was allowed to equilibrate after the CO_2 loading had been instantaneously doubled. In contrast, the HadGEM2-ES climate change simulation was a transient RCP8.5 run in which the radiative forcing was gradually increased, and so the atmospheric circulation is not expected to be in equilibrium with the contemporary radiative forcing. Therefore, the comparison is not strictly like for like. Nevertheless, the comparison shows for the first time that the projected increase in transatlantic turbulence is robust, because it occurs across multiple climate models and to first order it does not depend on the parameterized physics, model resolution, or greenhouse gas scenario. When the comparison is repeated after first downscaling the HadGEM2-ES wind and temperature fields to GFDL-CM2.1 resolution, before recomputing the MOG thresholds and recalculating the turbulence increases, the scatterplot is essentially unchanged.

Global geographic maps of the percentage change in the prevalence of moderate turbulence in the HadGEM2-ES simulations at 200 hPa in December, January, and February (DJF) are shown in Figure 2 for each of the 20 CAT indices. The percentage change refers to the period 2050–2080 compared to preindustrial times.

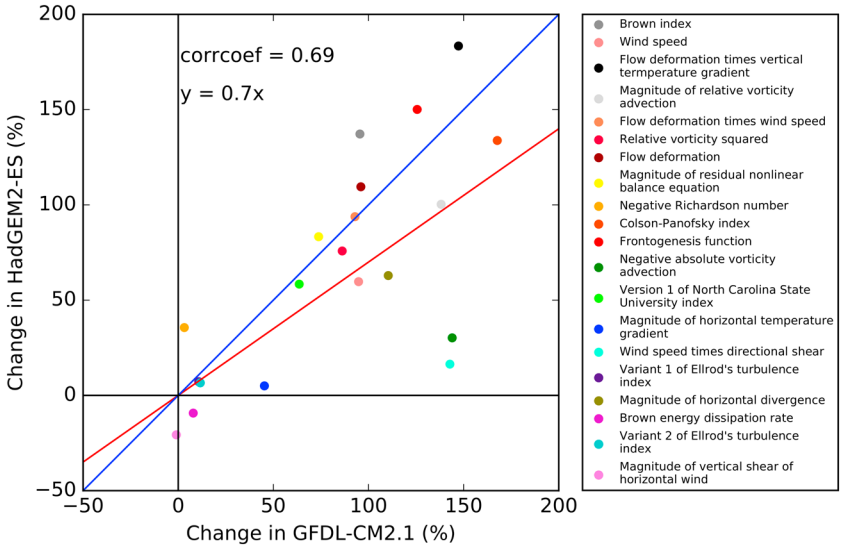

Figure 1. Scatterplot comparing the HadGEM2-ES simulations from the present study with the GFDL-CM2.1 simulations from Williams and Joshi (2013). The plot shows the percentage change in the prevalence of MOG turbulence for 20 CAT diagnostics calculated at 200 hPa over the north Atlantic (50–75°N and 10–60°W) in winter (December, January, and February; DJF). In this figure only, to ensure the fairest possible comparison, the HadGEM2-ES MOG thresholds are calculated from the control run in exactly the same way that the GFDL-CM2.1 thresholds were calculated by Williams and Joshi (2013), that is, using the 99th percentiles of CAT diagnosed from daily mean fields in the above geographic box and on the above pressure level in winter. The blue line ($y = x$) indicates parity and the red line ($y = 0.7x$) is a least-squares fit constrained to pass through the origin.

The indices are ranked in descending order according to the global-mean percentage change. (All geographic averages in this paper include the cosine(latitude) scaling factor, to downweight the smaller high-latitude grid boxes compared to the larger low-latitude ones.) Previous findings about CAT increasing in the North Atlantic evidently apply to other parts of the planet, too. In the tropical regions (30°S–30°N), the percentage changes are generally smaller and there is less agreement between the diagnostics. Outside the tropics, in the middle- and high-latitude regions, the percentage changes are generally larger and there is more agreement between the diagnostics.

To assess which features are robust among the different diagnostics, the 20 estimates of the percentage changes in CAT shown in Figure 2 for DJF are averaged and shown in the first panel of Figure 3. The remaining three panels in Figure 3 show the corresponding averages for March, April, and May (MAM), June, July, and August (JJA), and September, October, and November (SON). The averages being taken here are equally weighted, under the assumption that each of the 20 estimates is equally plausible. The percentage changes generally display relatively little seasonality, with the bulk spatial patterns occurring in all four seasons, although there does appear to be a moderate seasonal amplitude modulation locally in some regions. These bulk changes include large increases of several hundred per cent in the midlatitudes in both hemispheres. In the Southern Hemisphere, these increases peak at around 45–75°S and are fairly zonally symmetric. In the Northern Hemisphere, the increases peak at around 45–75°N but they display more zonal variability, which appears to be associated with the presence of land masses. The bulk features also include small and statistically insignificant decreases of several tens of per cent in parts of the tropics (where convection is a more important source of turbulence and CAT is less relevant). The global-mean percentage changes in moderate CAT at 200 hPa are +30.8% (DJF), +46.5% (MAM), +42.7% (JJA), and +39.2% (SON), where large increases in the midlatitudes are being partly offset by small decreases in the tropics.

The global-mean percentage changes for all five turbulence strength categories (light, light-to-moderate, moderate, moderate-to-severe, and severe) and both pressure levels (200 hPa and 250 hPa) in all four seasons (DJF, MAM, JJA, and SON) are tabulated in Table 1. In all 40 cases, the change is positive, indicating that CAT is intensifying across a range of strengths and altitudes and that it is intensifying throughout the year. The global-mean percentage changes are generally larger at 200 hPa than 250 hPa, largest for turbulence in the light strength category, and largest in MAM.

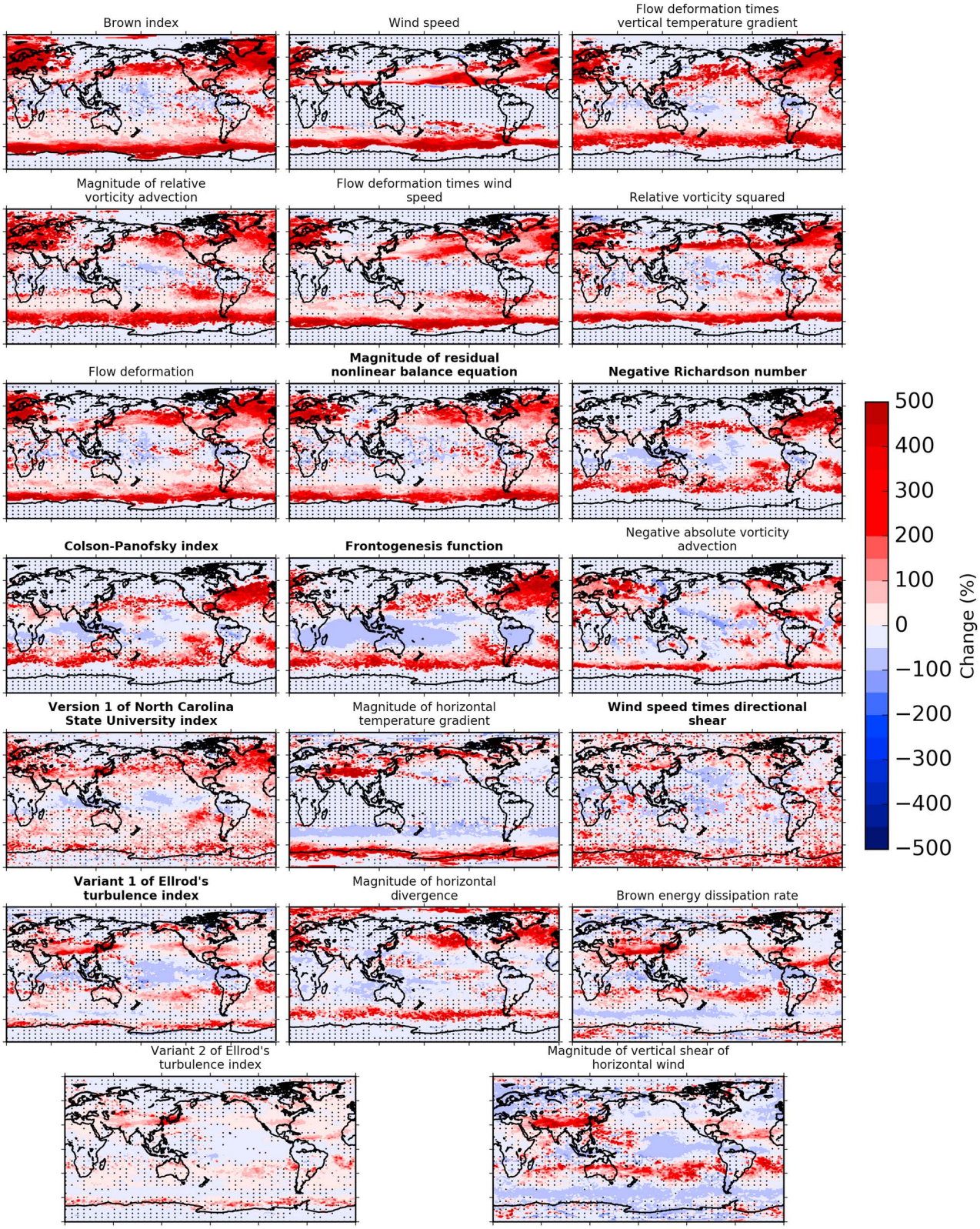

Figure 2. Maps of the percentage change in the amount of moderate CAT from preindustrial times (picontrol) to the period 2050–2080 (RCP8.5). The maps are calculated for all 20 CAT diagnostics at 200 hPa in December, January, and February (DJF) using the HadGEM2-ES climate model. The maps are ordered (from left to right and top to bottom) from the largest to smallest global-mean percentage change. Bold titles indicate the seven GTG2 upper-level diagnostics that are used operationally (Sharman et al., 2006). Stippling indicates regions where the percentage change is not statistically significant at the 90% level according to the two-tailed binomial test.

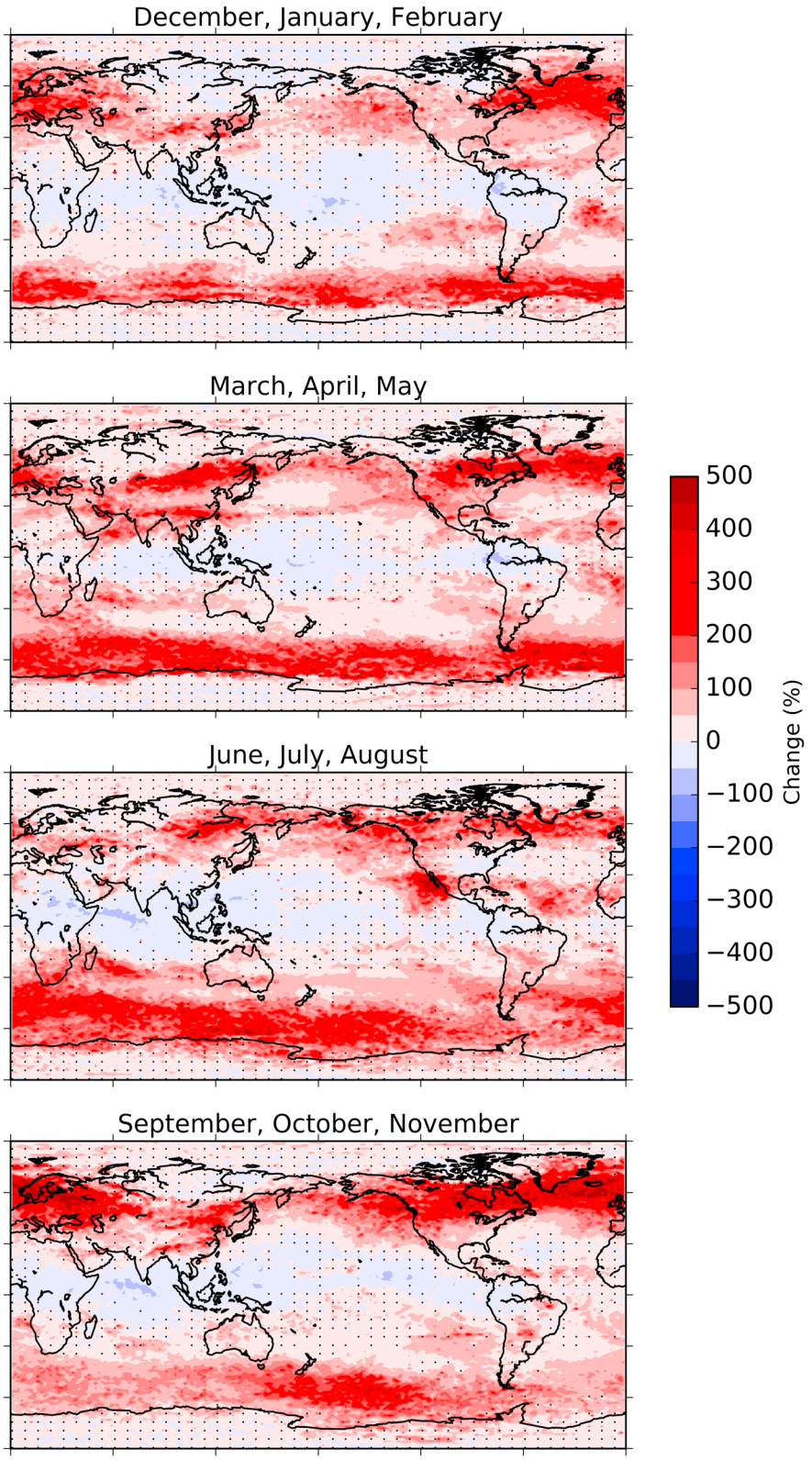

Figure 3. Maps of the average percentage change in the amount of moderate CAT from preindustrial times (picontrol) to the period 2050–2080 (RCP8.5) at 200 hPa in each season. The average is taken over all 20 CAT diagnostics, which are equally weighted. The upper panel for December, January, and February is the average of the 20 panels in Figure 2. Stippling indicates regions where the average percentage change is not significantly different from zero at the 90% level according to the one-sample, two-tailed *t* test.

Table 1
Global-Mean Percentage Changes in the Amount of CAT from Pre-Industrial Times (picontrol) to the Period 2050–2080 (RCP8.5)

Strength	DJF		MAM		JJA		SON	
Category	200 hPa	250 hPa	200 hPa	250 hPa	200 hPa	250 hPa	200 hPa	250 hPa
Light	+39.8	+23.2	+53.7	+32.3	+52.6	+31.8	+47.2	+26.6
Light-to-moderate	+35.9	+22.4	+53.4	+31.6	+51.4	+31.2	+45.9	+24.6
Moderate	+30.8	+19.6	+46.5	+30.0	+42.7	+28.3	+39.2	+23.5
Moderate-to-severe	+27.9	+17.5	+42.3	+28.0	+35.4	+25.3	+34.0	+21.4
Severe	+34.7	+20.5	+51.6	+34.2	+42.7	+29.8	+41.9	+25.5

Note. The changes are calculated for five turbulence strength categories, at two pressure altitudes, and in four seasons. The changes are averaged over 20 CAT diagnostics. DJF is December, January, and February; MAM is March, April, and May; JJA is June, July, and August; and SON is September, October, and November.

Because the above global averages mask large regional variations, Table 2 tabulates the annual-mean percentage changes averaged within eight geographic regions, for all five turbulence strength categories and both pressure levels. The results indicate that the busiest international airspace around the middle and high latitudes (North Atlantic, North America, North Pacific, Europe, and Asia) experiences larger increases in CAT than the global average, with the volume of severe CAT approximately doubling at 200 hPa over North America (+112.7%), the North Pacific (+91.6%), and Europe (+160.7%). The less congested skies around the tropics (Africa, South America, and Australia) generally experience smaller increases. Whereas globally, it is light turbulence that experiences the largest relative increase, locally, it can be severe turbulence (e.g., Europe). For each strength category and geographic region, the percentage change is larger at 200 hPa than 250 hPa. To provide some context to aid with the interpretation of the magnitudes of these changes, in the North Atlantic (50–75°N, 10–60°W) at 200 hPa, we find that (i) in winter, severe CAT by 2050–2080 will be as common as moderate CAT in the control period, and (ii) for a range of turbulence strengths from light to moderate-to-severe, summertime CAT by 2050–2080 will be as common as wintertime CAT in the control period.

Table 2
Annual-Mean Percentage Changes in the Amount of CAT From Pre-Industrial Times (picontrol) to the Period 2050–2080 (RCP8.5)

Strength	North Atlantic		North America		North Pacific		Europe	
Category	200 hPa	250 hPa	200 hPa	250 hPa	200 hPa	250 hPa	200 hPa	250 hPa
Light	+75.4	+47.3	+110.1	+71.0	+120.7	+82.0	+90.5	+59.9
Light-to-moderate	+124.1	+80.7	+113.6	+57.5	+106.6	+53.8	+130.7	+75.8
Moderate	+143.3	+74.4	+100.3	+50.2	+90.2	+41.6	+126.8	+60.8
Moderate-to-severe	+148.9	+71.0	+94.3	+47.0	+73.1	+35.3	+142.1	+66.1
Severe	+181.4	+88.0	+112.7	+58.9	+91.6	+40.1	+160.7	+90.6

Strength	South America		Africa		Asia		Australia	
Category	200 hPa	250 hPa	200 hPa	250 hPa	200 hPa	250 hPa	200 hPa	250 hPa
Light	+18.3	+13.4	+24.2	+18.9	+102.5	+65.1	+18.0	+9.5
Light-to-moderate	+27.1	+18.0	+27.9	+23.3	+92.4	+48.7	+23.1	+12.9
Moderate	+34.3	+22.8	+34.3	+26.0	+78.1	+48.7	+29.6	+19.1
Moderate-to-severe	+43.3	+23.8	+36.6	+26.9	+59.2	+47.9	+36.9	+24.8
Severe	+62.0	+31.6	+51.1	+40.2	+64.1	+55.4	+52.5	+35.4

Note. The changes are calculated for five turbulence strength categories, at two pressure altitudes, and within eight geographic regions. The changes are averaged over 20 CAT diagnostics. The geographic regions are: North Atlantic (50–75°N, 10–60°W), North America (25–75°N, 63–123°W), North Pacific (50–75°N, 145°E–123°W), Europe (35–75°N, 10°W–30°E), South America (55°S–10°N, 35–80°W), Africa (35°S–35°N, 15°W–50°E), Asia (10–75°N, 45–140°E), and Australia (12–46°S, 113–177°E).

4. Summary and Discussion

Using climate model simulations, this paper has found large relative increases in the atmospheric volume containing significant CAT by the period 2050–2080 under the RCP8.5 greenhouse gas forcing scenario. The increases occur throughout the global atmosphere but are most pronounced in the midlatitudes in both hemispheres. The increases occur in multiple aviation-relevant turbulence strength categories, at multiple flight levels, and in all seasons. We conclude that the intensification of CAT that has been calculated by previous studies, which considered only transatlantic flights in winter at altitudes of around 39,000 feet, apply more generally.

Our findings may have implications for aviation operations in the coming decades. Many of the aircraft that will be flying in the second half of the present century are currently in the design phase. It would therefore seem sensible for the airframe manufacturers to prepare for a more turbulent atmosphere, even at this early stage. Future aeronautical advances, such as remote sensing of clear-air turbulence using onboard light detection and ranging technology, might be able to mitigate the operational effects of the worsening atmospheric turbulence (Vrancken et al., 2016). Our results also reinforce the increasingly urgent need to improve the skill of operational CAT forecasts. Despite containing useful information and demonstrably improving the safety and comfort of air travel, these forecasts continue to include a substantial fraction of false positives and missed events.

Future research should extend our results by quantifying the remaining uncertainties. Although the present paper has captured uncertainties arising from gaps in our knowledge of turbulence generation by computing 20 different CAT diagnostics, two key sources of uncertainty remain unquantified. First, future emissions of greenhouse gases depend on socioeconomic and political factors. The corresponding uncertainty in CAT should be quantified by using other forcing scenarios in addition to the RCP8.5 scenario used herein. Second, the jet streams in the upper troposphere and lower stratosphere in different climate models may respond differently to a given radiative forcing anomaly. The corresponding uncertainty in CAT should be quantified by using other climate models in addition to the CMIP5 model used herein, such as the next generation of CMIP6 models that will have substantially higher spatial resolutions.

Future studies could also use a more recent historical period as the baseline, instead of the preindustrial control period. Turbulence reports from commercial aircraft could be used for climate model verification purposes. The grid resolution of numerical weather prediction models could be systematically degraded to match climate models, to assess how the turbulence diagnostics depend on resolution. Whereas the present study has investigated the climate response of clear-air turbulence, which is prevalent in the midlatitudes, future studies should investigate the climate response of convective turbulence, which is more prevalent in the tropics. Finally, the response of clear-air turbulence to natural climate variability, such as the North Atlantic Oscillation (Kim et al., 2016), also deserves further study.

Acknowledgments

L. N. S. acknowledges support through a PhD studentship from the Natural Environment Research Council SCENARIO Doctoral Training Partnership (reference NE/L002566). P. D. W. acknowledges support through a University Research Fellowship from the Royal Society (reference UF130571). For their roles in producing, coordinating, and making available the CMIP5 model output, we acknowledge the Met Office Hadley Centre, the World Climate Research Programme's (WCRP) Working Group on Coupled Modelling (WGCM), and the Global Organization for Earth System Science Portals (GO-ESSP).

References

Brown, R. (1973). New indices to locate clear-air turbulence. *Meteorological Magazine*, *102*, 347–361.

Chambers, E. (1955). Clear air turbulence and civil jet operations. *The Aeronautical Journal*, *59*(537), 613–628.

Coffel, E., & Horton, R. (2015). Climate change and the impact of extreme temperatures on aviation. *Weather, Climate, and Society*, *7*, 94–102.

Colson, D., & Panofsky, H. (1965). An index of clear air turbulence. *Quarterly Journal of the Royal Meteorological Society*, *91*(390), 507–513.

De Villiers, M., & van Heerden, J. (2001). Clear air turbulence over South Africa. *Meteorological Applications*, *8*(1), 119–126.

Ellrod, G. P., & Knapp, D. I. (1992). An objective clear-air turbulence forecasting technique: Verification and operational use. *Weather and Forecasting*, *7*(1), 150–165.

Flato, G., Marotzke, J., Abiodun, B., Braconnot, P., Chou, S. C., Collins, W. J., … Rummukainen, M. (2013). Evaluation of climate models. In T. F. Stocker et al. (Eds.), *Climate Change 2013: The Physical Science Basis. Contribution of Working Group I to the Fifth Assessment Report of the Intergovernmental Panel on Climate Change* (pp. 741–866). Cambridge, UK: Cambridge University Press.

Irvine, E. A., Shine, K. P., & Stringer, M. A. (2016). What are the implications of climate change for trans-Atlantic aircraft routing and flight time?, *Transportation Research Part D: Transport and Environment*, *47*, 44–53.

Irvine, E. A., Hoskins, B. J., Shine, K. P., Lunnon, R. W., & Froemming, C (2013). Characterizing North Atlantic weather patterns for climate-optimal aircraft routing. *Meteorological Applications*, *20*(1), 80–93.

Jaeger, E., & Sprenger, M. (2007). A Northern Hemispheric climatology of indices for clear air turbulence in the tropopause region derived from ERA40 reanalysis data. *Journal of Geophysical Research: Atmospheres* , *112*, D20106. https://doi.org/10.1029/2006JD008189

Jones, C., Hughes, J., Bellouin, N., Hardiman, S., Jones, G., Knight, J., … Zerroukat, M. (2011). The HadGEM2-ES implementation of CMIP5 centennial simulations. *Geoscientific Model Development*, *4*(3), 543–570.

Karnauskas, K. B., Donnelly, J. P., Barkley, H. C., & Martin, J. E (2011). Coupling between air travel and climate. *Nature Climate Change*, *5*, 1068–1073.

Kim, J.-H., & Chun, H.-Y. (2011). Statistics and possible sources of aviation turbulence over South Korea. *Journal of Applied Meteorology and Climatology*, *50*(2), 311–324.

Kim, J.-H., Chan, W. N., Sridhar, B., Sharman, R. D., Williams, P. D., & Strahan, M. (2016). Impact of the North Atlantic Oscillation on transatlantic flight routes and clear-air turbulence. *Journal of Applied Meteorology and Climatology*, *55*(3), 763–771.

Knox, J. A., McCann, D. W., & Williams, P. D. (2008). Application of the Lighthill–Ford theory of spontaneous imbalance to clear-air turbulence forecasting. *Journal of the Atmospheric Sciences*, *65*(10), 3292–3304.

Koch, S. E., & Dorian, P. B. (1988). A mesoscale gravity wave event observed during CCOPE. Part III: Wave environment and probable source mechanisms. *Monthly Weather Review*, *116*(12), 2570–2592.

Lane, T. P., Sharman, R. D., Trier, S. B., Fovell, R. G., & Williams, J. K. (2012). Recent advances in the understanding of near-cloud turbulence. *Bulletin of the American Meteorological Society*, *93*(4), 499–515.

Lilly, D. K. (1978). A severe downslope windstorm and aircraft turbulence event induced by a mountain wave. *Journal of the Atmospheric Sciences*, *35*(1), 59–77.

MacCready, P. B (1964). Standardization of gustiness values from aircraft. *Journal of Applied Meteorology*, *3*(4), 439–449.

McCann, D. W., Knox, J. A., & Williams, P. D. (2012). An improvement in clear-air turbulence forecasting based on spontaneous imbalance theory: The ULTURB algorithm. *Meteorological Applications*, *19*(1), 71–78.

Sharman, R., & Lane, T. (2016). *Aviation Turbulence: Processes, Detection, Prediction* (523 pp.). Switzerland: Springer.

Sharman, R., Tebaldi, C., Wiener, G., & Wolff, J (2006). An integrated approach to mid- and upper-level turbulence forecasting. *Weather and Forecasting*, *21*(3), 268–287.

Taylor, K. E., Stouffer, R. J., & Meehl, G. A (2012). An overview of CMIP5 and the experiment design. *Bulletin of the American Meteorological Society*, *93*(4), 485–498.

Tvaryanas, A. P. (2003). Epidemiology of turbulence-related injuries in airline cabin crew, 1992–2001. *Aviation, Space, and Environmental Medicine*, *74*(9), 970–976.

Uccellini, L. W., & Koch, S. E. (1987). The synoptic setting and possible energy sources for mesoscale wave disturbances. *Monthly Weather Review*, *115*(3), 721–729.

Van Vuuren, D. P., Edmonds, J., Kainuma, M., Riahi, K., Thomson, A., Hibbard, K., … Rose, S. K. (2011). The representative concentration pathways: An overview. *Climatic Change*, *109*, 5–31.

Vrancken, P., Wirth, M., Ehret, G., Barny, H., Rondeau, P., & Veerman, H. (2016). Airborne forward-pointing UV Rayleigh lidar for remote clear air turbulence detection: System design and performance. *Applied Optics*, *55*(32), 9314–9328.

Williams, P. D. (2016). Transatlantic flight times and climate change. *Environmental Research Letters*, *11*(2), 024008.

Williams, P. D. (2017). Increased light, moderate, and severe clear-air turbulence in response to climate change. *Advances in Atmospheric Sciences*, *34*(5), 576–586.

Williams, P. D., & Joshi, M. M. (2013). Intensification of winter transatlantic aviation turbulence in response to climate change. *Nature Climate Change*, *3*, 644–648.

Williams, P. D., & Joshi, M. M. (2016). Clear-air turbulence in a changing climate. Chapter 23 (pp. 465–480).. In R. Sharman, & T. Lane (Eds.), *viation Turbulence: Processes, Detection, Prediction* (523 pp.). Switzerland: Springer.

Williams, P. D., Haine, T. W. N., & Read, P. L. (2005). On the generation mechanisms of short-scale unbalanced modes in rotating two-layer flows with vertical shear. *Journal of Fluid Mechanics*, *528*, 1–22.

Williams, P. D., Haine, T. W. N., & Read, P. L. (2008). Inertia–gravity waves emitted from balanced flow: Observations, properties, and consequences. *Journal of the Atmospheric Sciences*, *65*(11), 3543–3556.

Williams, P. D., Read, P. L., & Haine, T. W. N. (2003). Spontaneous generation and impact of inertia–gravity waves in a stratified, two-layer shear flow. *Geophysical Research Letters*, *30*(24), 2255. https://doi.org/10.1029/2003GL018498